Tungsten−Doped TiO2 vs Pure TiO2 Photocatalysts: Effects on Photobleaching Kinetics and Mechanism

ARTICLE *in* THE JOURNAL OF PHYSICAL CHEMISTRY C · JANUARY 2008

Impact Factor: 4.77 · DOI: 10.1021/jp0769781

4 AUTHORS, INCLUDING:

Fernando García Einschlag
National University of La Plata
33 PUBLICATIONS **475** CITATIONS
SEE PROFILE

Matías Jobbagy
University of Buenos Aires
91 PUBLICATIONS **1,395** CITATIONS
SEE PROFILE

Tungsten-Doped TiO_2 vs Pure TiO_2 Photocatalysts: Effects on Photobleaching Kinetics and Mechanism

Natalia Couselo,[†] Fernando S. García Einschlag,[‡] Roberto J. Candal,[†] and Matías Jobbágy*[,†]

INQUIMAE, Facultad de Ciencias Exactas y Naturales, Universidad de Buenos Aires, Pabellón II, Ciudad Universitaria, C1428EHA-Buenos Aires, Argentina, and INIFTA, Departamento de Química, Facultad de Ciencias Exactas, Universidad Nacional de La Plata, Casilla de Correo 16, Sucursal 4, (1900), La Plata, Argentina

Received: August 30, 2007; In Final Form: October 18, 2007

Sol gel prepared tungsten (VI) doped TiO_2 powders were evaluated as photocatalysts for crystal violet (CV) bleaching under UV irradiation, in the presence of oxygen. The incorporation of the hexavalent cation affects both surface and bulk properties. The optimum activity observed results from the competition between higher surface areas and lower specific activities per adsorption site. At pH 4.0, doped particles share a common photodegradation mechanism, where the relative contribution of the aromatic structure rupture over the loss of terminal methyl groups (N-demethylation) is more relevant than in the case of non-doped titania. This behavior can be minimized shifting the pH into basic condition.

1. Introduction

TiO_2-based photocatalysts arise as some of the most promising agents for the decomposition of organic pollutants present in waters or air.[1] To enhance the photocatalytic activity in the visible range, several transition-metal-doped TiO_2 were synthesized.[2,3] The incorporation of a foreign cation within TiO_2 affects both surface and bulk properties. In the case of W(VI), this cation tends to migrate toward the surface, shifting the isoelectric point to lower values, in comparison to pristine TiO_2.[4] Bulk properties are also modified because of the isomorphic substitution within the lattice; the electronic properties of the doped material are notably different when compared with the pristine oxide.[5] The W(VI) surface clusters work as electron traps, which lead to photochromic materials with energy storage capacity.[6,7] In principle, the presence of W(VI) could improve the photodegradation ability of TiO_2 in several ways.[8] It prevents the recombination of the electron−hole pairs[9] as well as expands the range of useful excitation light to the visible spectra. In addition, the chemical changes of the surface result in enhanced acidity.[10] The relative weight of each one of those factors is the subject of current discussion.[11] Taking into account the aforementioned factors, the photodegradation mechanism can be affected when W(VI) is incorporated into the catalyst.

Certain aromatic dyes such as crystal violet (CV) exhibit two main mechanisms of photodegradation. One path involves the consecutive departure of terminal methyl groups (N-demethylation) while the aromatic structure of the molecule is preserved. In that process, a complete transformation of CV into fuchsine basic (FB) takes place, with an absorption maximum displacement from 590 to 540 nm (see structures of both compounds in the Supporting Information).[12,13] The other path involves the rupture of the conjugated structure, producing the instant bleaching of aromatic dyes. Then, CV arises as a suitable probe to follow the competition between the N-demethylation over the disruption of the conjugated structure. The study of basic aspects of aromatic dyes photocatalytic degradation contributes to the optimization of wastewater remediation technologies. The aim of the present work is to evaluate and discuss how the tungsten loading on titania affects the rate and mechanism of CV photocatalytic decomposition. To minimize the photosensitizer effect of CV, a UV light source ($\lambda = 350$ nm) was employed to generate the electron−hole pairs.[14]

2. Experimental Procedure

2.1. Materials. Titanium (IV) isopropoxide (99%) and crystal violet (>90%) were purchased from Aldrich. Nitric acid was purchased from Mallinckrodt. Ammonium metatungstate was prepared in the laboratory by neutralization of tungsten acid with ammonia.

2.2. Synthesis of TiO_2-Based Photocatalysts. Pure TiO_2 and 0.5, 2.0, 4.5, and 6.0% mol/mol tungsten-doped TiO_2 were prepared by a sol−gel process. Samples were named as *X*W, where *X* indicates the percentage of W atoms with respect to the total cationic content. The necessary amounts of $(NH_4)_{10}W_{12}O_{41}{\cdot}7H_2O$ were dissolved in 180 mL of water containing 1.8 mL of concentrated nitric acid contained in an open spherical flask. Fifteen milliliters of titanium isopropoxide was slowly incorporated to the acid solution under strong agitation. A white precipitate was obtained immediately. The suspension was heated at 80 °C in the open flask for 30 min; the alcohol produced as consequence of the alcoxide hydrolysis was partially evaporated in this step. Finally, the suspension was refluxed at 80 °C for 2 h until total peptization. The obtained sol was poured in polypropylene weighting dishes and dried at 40 °C in an oven. Light-yellow xerogels were obtained after drying. The "chips" were ground in an agate mortar until a yellowish powder was obtained. The powders were fired at 500 °C for 5 h with a 5 °C min^{-1} ramp.

The crystalline structure of the solids was determined by powder X-ray diffraction (PXRD) analysis (Siemens D-5000). The surface area of the powders was determined by nitrogen adsorption, following the BET approach (Gemini 2360 V2). To

* Corresponding author. E-mail: jobbag@qi.fcen.uba.ar.
[†] INQUIMAE.
[‡] INIFTA.

10.1021/jp0769781 CCC: $40.75
Published on Web 01/08/2008

determine the electrophoretic mobility of the oxides (Brookhaven 90-Plus), the powders, previously sieved through a 400 platinum mesh, were suspended in a 1 mM solution of KCl. The pH was adjusted with HNO_3 or NaOH. The morphology and composition of the particles was determined by scanning electron microscopy (SEM) and energy-dispersive analysis (EDS) probe (Philips SEM 515).

2.3. Adsorption of CV on the Photocatalysts. To determine the adsorption isotherms of CV on the photocatalysts at pH 4.0, 7.0, or 9.0, we prepared 1.00 g/L suspensions of the powders in water containing the desired amount of CV. The pH was adjusted with NaOH or $HClO_4$ solutions. The solids were removed after 3 h of continuous stirring by ultracentrifugation at 12 750 rpm; previous experiences revealed that sorption equilibrium is reached in these conditions. The concentration of the bulk solution in equilibrium with the solids was determined by UV−vis spectroscopy (Hewlett-Packard HP4511). The amount of CV adsorbed on the solids was calculated from the difference between the total and equilibrium concentrations of CV.

2.4. Photocatalytic Degradation of CV. All of the kinetic runs were performed using 35.5 mg/L CV solutions with a photocatalyst content of 1.00 g/L, oxygen bubbling, and the initial pH fixed at the desired value. Previous to irradiation, the suspensions were shaken for 3 h in order to reach the adsorption equilibrium. Experiments were performed in a cylindrical borosilicate glass made reactor, with capacity for 125 mL. Seventy-five milliliters of a suspension containing 1.00 g/L of photocatalyst and 35 mg/L of CV were placed in the reactor. The suspension was magnetically stirred and oxygen bubbled during the experiment. The reactor was illuminated with UV light provided by four black light tubes (8 W F8T5BLB,-PHILIPS), symmetrically placed around the cylinder. A distance of 5 cm separated the tubes from the external wall of the reactor. The temperature of the solution was maintained at 30 °C with the help of two coolers placed at the sides of the reactor. The pH of the suspensions was adjusted in the dark to the desired value with NaOH or $HClO_4$ previous to the photocatalytic experiment. The pH was adjusted until a constant reading was observed for at least 20 min. To ensure that equilibrium was reached, the suspension was stirred in the dark for another 20 min. One milliliter sample was taken from the reactor every 10 min and stored in Eppendorf tubes. The solids were removed by centrifugation at 12 750 rpm. Changes in the dye concentration were determined by UV−visible spectroscopy (Hewlett-Packard HP4511). Discoloration kinetics of CV was determined by plotting the absorbance decay (normalized to the initial absorbance) as a function of time. Certain solutions extracted at different reaction times were separated from the photocatalysts and evaporated under vacuum. The remaining solids were dissolved in deuterated dymethylsulfoxide (DMSO-Aldrich) and characterized by ^1H NMR.

Control experiments were performed by the UV illumination of aqueous solutions containing 35.5 mg/L CV at pH 4.0 for 3 h in the absence of titania. Other control experiments were performed by dispersing the titania catalyst (1.00 g/L) in a solution containing 35.5 mg/L CV in the absence of light. In both cases, no changes in the absorption spectrum were observed.

To estimate the contribution of the species formed during the photodegradation experience to the total absorbance, we applied an alternating least-squares (ALS) routine to describe the observed spectra as the partial contribution of CV, a generic partially demethylated dye, and the end product, FB. This method is based on the resolution of the experimental data matrix, $\mathbf{A}(t \times w)$ into matrices $\mathbf{C}$ and $\mathbf{S^T}$, by the iterative application of the following matrix product: $\mathbf{A} = \mathbf{CS}^T + \mathbf{E}$ where $\mathbf{C}(t \times n)$ is the kinetic profile matrix; $\mathbf{S}^T(n \times w)$ is that containing the spectral profiles, and $\mathbf{E}(t \times w)$ represents the error matrix. Symbols t, n, and w denote the sampling times, the number of absorbing species, and the recorded wavelengths, respectively.[15]

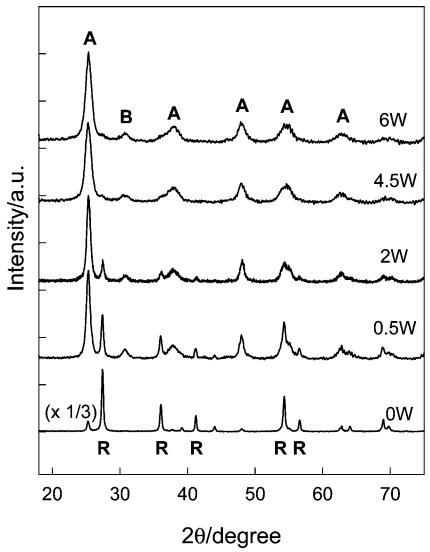

Figure 1. PXRD patterns for samples annealed at 500 °C for 5 h, with increasing tungsten contents. Peaks pointed as A, B, or R correspond to anatase, brookite, and rutile, respectively.

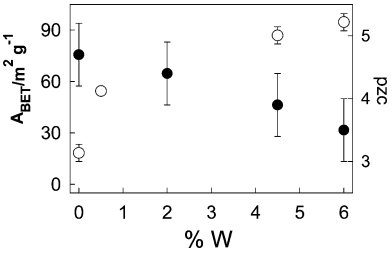

Figure 2. BET surface area (○) and point of zero charge (●) as a function of tungsten content.

3. Results and Discussion

3.1. Characterization of the Photocatalysts. Figure 1 shows the PXRD patterns of samples loaded with different amount of tungsten, annealed for 3 h at 500 °C. The sample 0W shows the coexistence of rutile and anatase. When tungsten is incorporated to TiO_2, the aforementioned phases coexist with Brookite, as evidenced by a reflection centered at 31°. The presence of this phase in related systems was noticed by previous explorations based on Raman spectroscopy.[10,18] The PXRD patterns revealed that as the amount of tungsten increased the samples became richer in anatase while the diffraction peaks turned broader, indicating smaller crystal sizes. Several authors have described similar behavior when tungsten is incorporated in TiO_2.[19] It was suggested that tungsten concentrates on the surface of the TiO_2 grains, hindering both the crystal growth and anatase to rutile transition.[20,21] Tungsten oxide or other crystalline forms of tungsten compounds were not detected; it was reported that only after annealing at temperatures as high as 1000 °C can the segregation of crystalline tungsten oxide be observed by conventional PXRD.[22] Figure 2 shows the surface areas determined by BET analysis and the isoelectric point of

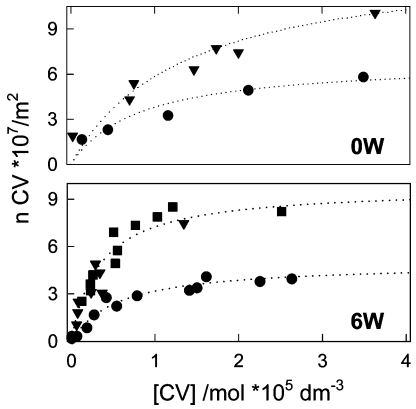

Figure 3. Adsorption isotherms (normalized to the surface area per gram of solid) of CV over non-doped (0W) and doped (6W) samples, at 298 K and pH values of 4.0 (●), 7.0 (▼), and 9.0 (■).

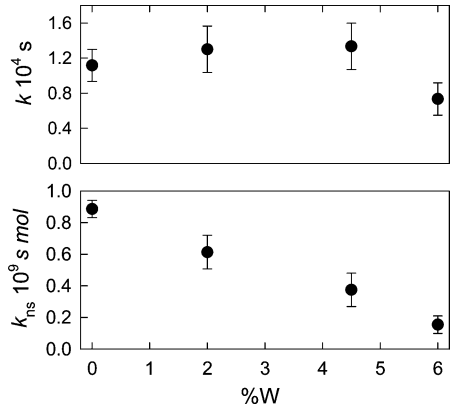

Figure 4. Apparent bleaching constant, observed at pH 4.0, as a function of tungsten content (upper view) and the same constant referred to the maximum adsorption capacity (lower view) of each photocatalyst.

samples with different amount of tungsten. In agreement with the PXRD results, the surface area increases with the amount of tungsten. The diminution in the zpc indicates that at least part of the tungsten incorporated to the material is placed on the surface. Tungsten (VI) oxides are more acidic than Ti(IV) oxides, so its presence on the surface increase the number of Brønsted acid sites,[23] reducing the isoelectric point.[24] Despite the fact that both the BET surface area and the zpc are affected by W loading, the surface area seems to be more sensitive than zpc to the amount of tungsten. The chemical stability of the employed photocatalyst was assessed by SEM-EDS inspection; the constancy of W/Ti ratios before and after photocatalytic experiments revealed that these binary oxides are stable toward W(VI) lixiviation.

3.2. Adsorption of CV onto W−TiO_2 Surfaces. To evaluate the effect of tungsten load on the TiO_2 adsorption capacity for CV, several adsorption experiments were performed in the dark.[25] Incorporation of W(VI) onto TiO_2 produced a notable increment in the amount of CV adsorbed by photocatalyst unit mass (at pH 4.0 the amount of CV adsorbed per gram of photocatalyst is 10 times higher when 6% mol/mol of W(VI) is incorporated to TiO_2). However, as is shown in Figure 3, once the number of CV molecules is normalized to the surface area, the sorption capacity remains constant for all samples. Thus, the increase in the amount of CV adsorbed on the W(VI) doped TiO_2 is a consequence of the enhancement of the surface area.

Figure 3 also shows that in both cases by increasing the pH from 4.0 to 7.0 the adsorption of CV approximately doubles, indicating that other surface sites or adsorption modes are

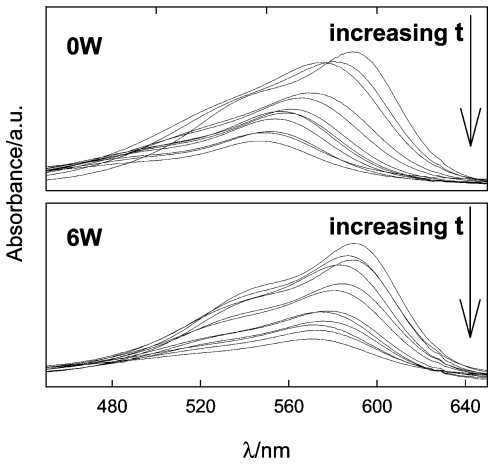

Figure 5. Evolution of partially degraded, at pH 4.0, CV solutions spectra, as a function of time over non-doped (0W, upper view) and doped (6W, lower view) catalysts.

available at the higher pH. However, when the pH increases to 9.0, sample 6W does not improve sorption of CV. Then, the sorption capacity reached at pH 7.0 can be considered the true maximum sorption capacity.

3.3. Photocatalytic Degradation of CV. *3.3.1. Effect of Tungsten Load on W−TiO_2 Photocatalytic Activity.* For all of the samples, discoloration kinetics can be fitted with a pseudo-first-order kinetic in terms of the commonly used Langmuir−Hinshelwood approach, as was reported previously for related systems.[26] Although this simple model is blind to the complexity involved in this kind of heterogeneous photoreactions,[27,28] is a useful tool for comparison purposes, allowing the obtention of an apparent bleaching constant for each experimental condition.[25] Xu and Landford,[29] after an intense study on the photocatalytic degradation of the red dye X3B, concluded that the rate in the bulk solution could be used as a measure of the photoactivity among different photocatalysts.

Previous reports indicate that W(VI) loaded TiO_2 catalysts maximize their photodegradation rate when the degree of atomic substitution lies between 1.7 and 4%, depending on the preparation procedures.[30−32] Figure 4 (upper view) plots the apparent bleaching constant as a function of W content. In accordance with previous reports, the photocatalytic activity (bleaching rate constants) reaches a maximum in the studied interval, around 3% in W atoms. However, those samples exhibited both increasing areas and sorption capacities with increasing W contents. The sorption capacity of each sample was calculated using Langmuir linearization of the corresponding sorption isotherms. As shown in Figure 4 (lower view), once the rate constants of each sample are corrected by the amount of effective adsorption sites, a strictly decreasing behavior is observed. In other words, the adsorption sites tend to be less active with increasing W content. Then, the observed maximum in the photocatalytic activity results from the competition between increasing sorption capacity and decreasing specific activity of each adsorption site. In other words, the contribution of tungsten loading toward improvement of the activity of TiO_2-based photocatalysts is to preserve the surface area during the thermal treatment of the oxides.

3.3.2. Evolution of CV during Photocatalysis; Influence of W. Figure 5 (upper view) shows the evolution of absorption spectra of the supernatant solution as a function of irradiation time, in the presence of 0W photocatalyst, at pH 4.0. The curve at zero time shows the visible spectrum of CV, with the characteristic maximum centered at 590 nm. For longer irradia-

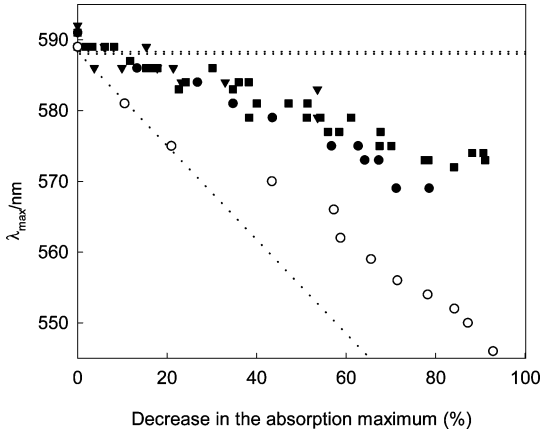

Figure 6. Mechanism plot for CV photodegradation runs performed at pH 4.0 over 0W (○), 2W (●), 4.5W (▼), and 6W (■) photocatalysts. Horizontal dotted line represents the bleaching path in the absence of N-demethylation while the tilted line represents the N-demethylation path in the absence of aromatic structure cleavage.

tion times, the absorption peak decrease with a hypsochromic shift from 590 to 550 nm, evidenced by a color change from violet to red-violet. In the presence of 6W photocatalyst, the shift is much less pronounced (Figure 5 lower view); for all of those samples the maximum shift decreases to about 20 nm.

Figure 6 shows the hypsochromic change of the absorption maximum (related to demethylation reaction) against the relative absorbance decay or bleaching (related to aromatic structure rupture).[33] These time-independent plots were chosen in order to allow a straight comparison of the relative weight of one degradation path over the other, for the different runs, irrespective of their bleaching rate. The plots also expose the two limit cases in the form of dotted lines. The tilted line represents total N-demethylation in the absence of aromatic ring rupture; the slope of this line is constrained by the maximum absorption shift and absorbance decay involved in the complete transformation of CV into FB.[14] The horizontal line represents the opposite behavior in which ring rupture is much faster than N-demethylation. All of the doped samples behave in a similar way, with a lower contribution of N-demethylation than the 0W sample. Then, a detailed analysis of spectra evolution as a function of irradiation time (see the Experimental Section) was performed through the comparison of two extreme cases: 0W and 6W photocatalysts. After the ALS analysis, interesting differences can be noted. In the case of the non-doped titania, the spectral evolution can be described as the contribution of CV, BF, and a generic partially demethylated intermediate, *X*, with an absorbance maximum placed at 565 nm (Figure 7). This intermediate considers the average contribution of the eight partially demethylated byproducts of CV. However, when tungsten-loaded photocatalysts are used, the spectra of the remaining solution can be described as the contribution of the initial CV and a partially demethylated intermediate *Y*, only. The maximum of absorbance for *Y* is placed at 575 nm, which indicates a lower degree of demethylation than *X*. According to the recent findings of Chen et al.,[12] in this case CV molecules typically lost less than three methyl groups before their aromatic cleavage. Figure 8 shows the temporal evolution of the different species in irradiated systems containing TiO_2 or tungsten-loaded TiO_2 photocatalysts, calculated from the ALS analysis. When pure TiO_2 is used as a photocatalyst (Figure 8 upper view), the concentration of *X* reached a maximum at ca. 150 min, while the concentration of BF increases monotonically after ca. 30 min of irradiation. These results suggest that BF is produced at expenses of *X*; longer irradiation times probably lead to BF

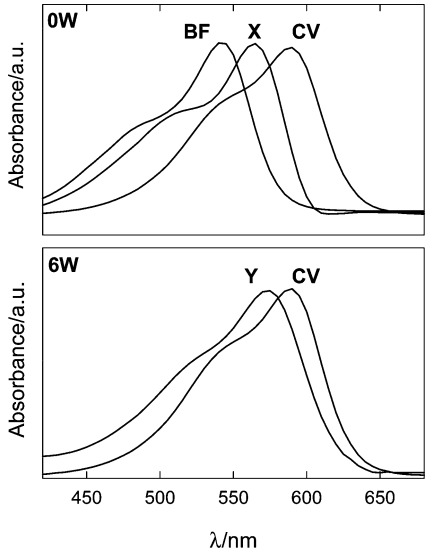

Figure 7. Extracted spectra from the partially degraded CV solutions over non-doped (0W, upper view) and doped (6W, lower view) samples. Intermediate species X and Y correspond to the spectral contribution of the involved partially demethylated dyes; CV and FB correspond to the end members crystal violet and fuchsin basic, respectively.

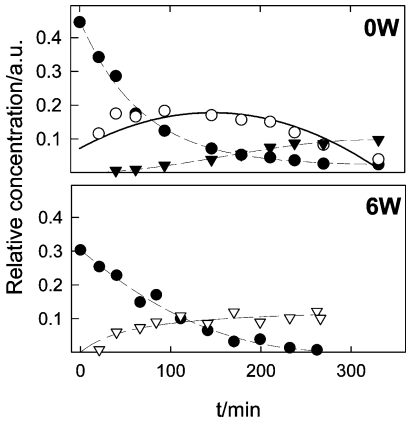

Figure 8. Concentration evolution of CV (●), intermediate X (○), FB (▼), and intermediate Y (▽) as a function of photodegradation time over doped (6W) and non-doped sample (0W), at pH 4.5, obtained from ALS analysis. Dotted lines are for visualization purposes.

degradation. When the doped photocatalysts were used (Figure 8, lower view), intermediate *Y* was rapidly produced at the beginning of the process, but its concentration stabilizes after 120 min of irradiation.

To confirm the reaction mechanism developed with both photocatalysts, we characterized the byproducts formed at different irradiation times (at pH 4.0) by ^{1}H NMR (see Figure 9). The sampling times were chosen based on the profiles shown in Figure 8. In the case of sample 0W, with increasing irradiation time, the intensity of the signal corresponding to the methyl group: $-N(CH_3)_2$ ($\delta = 3.2$) decreased and almost disappeared. Simultaneously, a transient signal at $\delta = 2.9$ was observed; this signal probably corresponded to $-NH(CH_3)$ methyls. The proton signals of the aromatic rings changed radically during the irradiation process, from two doublets centered at $\delta = 7.00$ and $\delta = 7.29$ (which correspond, to aromatic H place in the ortho or metha position from the amine group, respectively) to a complex family of peaks in the range $6.8 < \delta < 7.8$. The former peaks split into the latter because of the loss of symmetry of the eight partially N-demethylated forms. In addition, signals in the range 4.4−5.2, which correspond to $Ar-NH_2$, were also observed. Aromatic ring opening was revealed by the occurrence

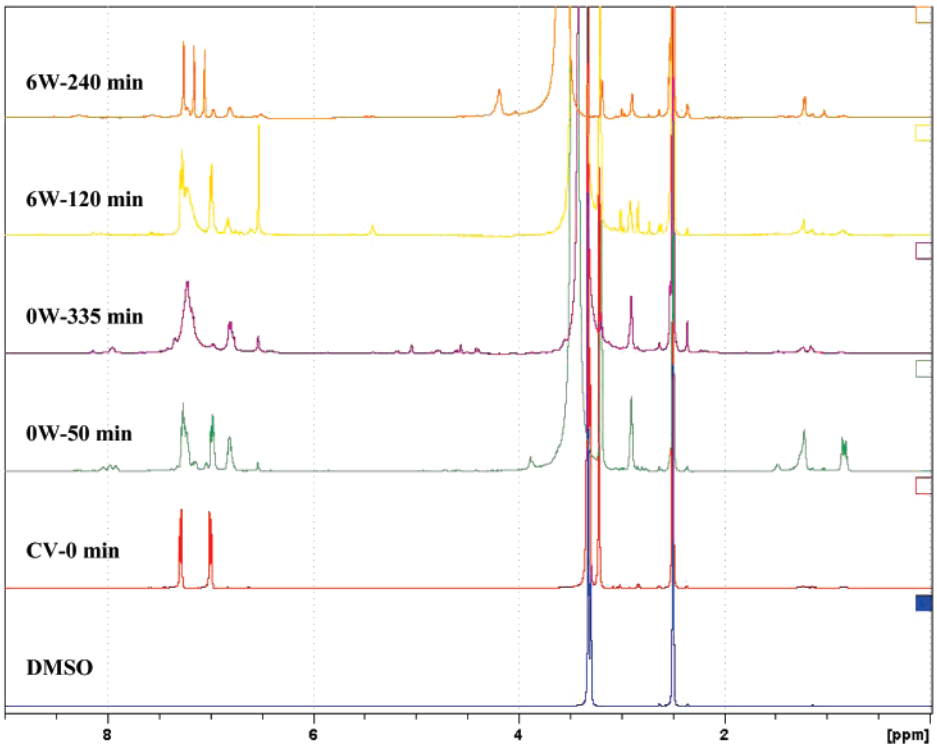

Figure 9. ^{1}H NMR spectra of CV (solid line) of partially degraded CV solutions (at pH 4.0) over doped (6W) and non-doped (0W) samples as a function of time. The spectrum of the deuterated dimethylsulfoxide (DMSO) employed as extraction solvent is also presented.

of peaks in the range $0.8 < \delta < 1.2$, which corresponded to aliphatic CH_n. Some peaks observed at high δ values ($\delta \geq 7.98$) are related to the presence of oxidized byproducts, as phenol or formic acid. These results confirm that in the studied degradation process of CV the N-demethylation coexists with the opening of the aromatic skeleton. In the case of the 6W sample, the most important difference lies in the low intensity of the peaks centered at $\delta = 2.9$ ($-NH(CH_3)$). In addition, the diminution of the peaks corresponding to aromatic H ($6.5 < \delta < 7.5$) and the simultaneous increment of the intensity of the peaks corresponding to alkyl H ($0.8 < \delta < 1.2$) indicate the opening of the ring during irradiation. Some features corresponding to high oxidation byproducts, such as HCOOH ($\delta = 8.2$), are also identified in the spectra. These results support the information obtained by UV−visible spectroscopy, which indicate that N-demethylation is not the main degradation pathway when 6W is used as photocatalyst.

3.3.3. Role of pH on CV Degradation Rate and Mechanism. The pH has a noticeable effect when the run of 6W sample is repeated at pH 7 and 9. As shown in Figure 10, basic conditions enhance the role of N-demethylation in the overall reaction. Interestingly, at those pH values, the surface of 6W is negatively charged and CV sorption capacity is almost equal (see Figures 2 and 3). These results suggest that the surface coverage (or adsorption mode) is not the factor that induces the mechanism modification, as was reported for other dyes.[34] Besides, the overall bleaching rate remains almost constant in the pH range 4.0−9.0; this fact suggests that the initial CV coverage of the surface is not a rate-determinant factor under the studied conditions.

3.3.4. General Aspects of the Degradation Mechanism. When CV is irradiated with visible light, in the presence of O_2 and TiO_2, the excited dye transfers an electron to the conduction band of the semiconductor; the electron transfer from this band to adsorbed oxygen results in the generation of superoxide ($O_2^{\bullet-}$) radical.[14] It was suggested that such reactive oxygen species

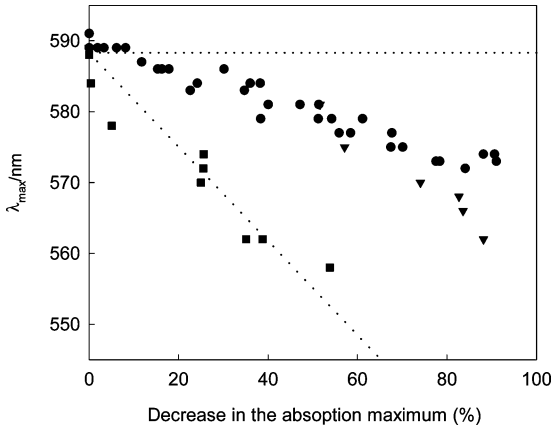

Figure 10. Mechanism plot for CV photodegradation runs performed over a 6W sample at pH 4.0 (●), pH 7.0 (▼), and pH 9.0 (■). Horizontal dotted line represents bleaching in the absence of N-demethylation while the tilted line represents N-demethylation in the absence of aromatic structure cleavage.

can cause cleavage of the aromatic structure of the remaining CV radical cation, at diffusion controlled rates, favoring the straight bleaching reaction.[35,36] In the present case, UV excitation triggers the generation of a hole−electron pair in the solid (eq 1). This first event simultaneously triggers the generation of $O_2^{\bullet-}$ and $OH^{\bullet}$ radicals (eqs 2 and 4). It is well established that $OH^{\bullet}$ radicals react with aromatic rings by successive additions leading finally to ring-opening products (eq 9). However, as was suggested recently, $O_2^{\bullet-}$ can give both *N*-de-alkylation and chromophore destruction products by reacting with the dye or its radical cations, and this subject is still matter of discussion.[37,38] Concerning doped titanias, it was reported that metal ions and polyoxometalates (e.g., polyphosphotungstates) adsorbed onto TiO_2 surfaces are able to capture the conduction band electrons, hindering $O_2^{\bullet-}$ generation.[39,40] In the present work, the surface W(VI) clusters present in the doped samples could play this role (eq 5), diminishing the production of $O_2^{\bullet-}$

(eq 4). The inhibition of superoxide radical pathways (eqs 10 and 11) results in a higher contribution of the $OH^\bullet$ pathways (eq 9), thereby leading to ring-opening products.

Concerning the role of pH in the mechanism, low proton concentrations prevent the $O_2^{\bullet-}$ transformation into H_2O_2 (eqs 6 and 7) and the subsequent generation of secondary $OH^\bullet$ (eq 8). Then we can expect to find an enhancement of superoxide-mediated reactions (eqs 10 and 11) at high pH values. It is worth mentioning that the conditions that favor superoxide production favor the N-demethylation pathways, whereas in conditions where superoxide is depressed ring opening prevails. These results might suggest that $O_2^{\bullet-}$ is rather involved in dealquilation than ring-opening reactions.

$$TiO_2 + h\nu\ (UV) \rightarrow TiO_2(h^+) + TiO_2(e_{cb}^-) \quad (1)$$

$$TiO_2(h^+) + OH^- \rightarrow OH^\bullet \quad (2)$$

$$TiO_2(h^+) + Dye \rightarrow Dye^{\bullet+} \quad (3)$$

$$TiO_2(e_{cb}^-) + O_2 \rightarrow O_2^{\bullet-} \quad (4)$$

$$TiO_2(e_{cb}^-) + W(VI) \rightarrow W(V) \quad (5)$$

$$O_2^{\bullet-} + TiO_2(e_{cb}^-) + 2H^+ \rightarrow H_2O_2 \quad (6)$$

$$2\ O_2^{\bullet-} + 2H^+ \rightarrow H_2O_2 + O_2 \quad (7)$$

$$H_2O_2 + TiO_2(e_{cb}^-) \rightarrow OH^\bullet + OH^- \quad (8)$$

$$OH^\bullet + Dye/Dye^{\bullet+} \rightarrow \rightarrow \rightarrow \text{ring opening} \quad (9)$$

$$O_2^{\bullet-} + Dye/Dye^{\bullet+} \rightarrow \text{N-demethylation} \rightarrow \rightarrow FB \quad (10)$$

$$O_2^{\bullet-} + Dye/Dye^{\bullet+} \rightarrow \rightarrow \rightarrow \text{ring opening} \quad (11)$$

4. Conclusions

Both the nature of TiO_2 surface and bulk properties and the photocatalytic reactivity are modified by the incorporation of W(VI). The stability of the anatase phase and the specific surface area during thermal treatment is enhanced. The presence of W(VI) on the surface of the material decreases the pzc of the particles, while the CV sorption capacity mainly depends on the surface area and pH, irrespective of the W(VI) content. Depending on the pH, at least two kinds of adsorption sites (or modes) are observed, over doped or pure titania. Photocatalytic degradation of CV can be accomplished on pure and tungsten-doped TiO_2, exhibiting in both cases pseudo-first-order bleaching rate law. The highest bleaching rate per gram of photocatalyst is the result of a competition between the surface area and the intrinsic bleaching activity of each adsorption site, exhibiting a maximum around 3% in W content.

At pH 4.0, all of the doped samples exhibit a common pathway in which N-demethylation has a lower efficiency (in relation to aromatic structure rupture) than that observed over pure TiO_2. The reaction mechanism also depends on the suspension pH; N-demethylation is favored at higher pH. The modification of the reaction path by incorporation of transition-metal cations on TiO_2, as well as pH control, may have important implications in the aim of achieving more specific cleavage of undesired aromatic structures.

Chemometric analysis of spectral evolution allowed us to extract mechanistic information in a simple way without the need for expensive separation steps.

Acknowledgment. This work was supported by the CONICET PIP 5215 project and PICT 06-10621. R.J.C, F.G.E., and M.J. are members of CONICET. F.G.E. thanks the financial support provided by Fundación Antorchas under Project No. 4248-70. We are indebted to Professor Favalli (UNLP) is for his helpful discussions.

Supporting Information Available: The molecular structures of crystal violet and basic fuchsine. This material is available free of charge via the Internet at http://pubs.acs.org.

References and Notes

(1) Hoffmann, M. R.; Martin, S. T.; Choi, W.; Bahnemann, D. W. *Chem. Rev.* **1995**, *95*, 69−96.
(2) Choi, W.; Termin, A.; Hoffmann, M. R. *J. Phys. Chem.* **1994**, *98*, 13669−13679.
(3) Fuerte, A.; Hernández-Alonso, M. D.; Maira, A. J.; Martínez-Arias, A.; Fernández-García, M.; Conesa, J. C.; Soria, J. *Chem. Commun.* **2001**, 2718−2719.
(4) Li, X. Z.; Li, F. B.; Yang, C. L.; Ge, W. K. *J. Photochem. Photobiol., A* **2001**, *141*, 209−217.
(5) Fernández-García, M.; Martínez-Arias, A.; Fuerte, A.; Conesa, J. C. *J. Phys. Chem. B* **2005**, *109*, 6075−6083.
(6) Alcober, C.; Alvarez, F.; Bilmes, S. A.; Candal, R. J. *J. Mater. Sci. Lett.* **2002**, *21*, 501−504.
(7) Tatsuma, T.; Saitoh, S.; Ngaotrakanwiwat, P.; Ohko, Y.; Fujishima, A. *Langmuir* **2002**, *18*, 7777−7779.
(8) Fuerte, A.; Hernández-Alonso, M. D.; Iglesias-Juez, A.; Martínez-Arias, A.; Conesa, J. C.; Soria, J.; Fernández-García, M. *Phys. Chem. Chem. Phys.* **2003**, *5*, 2913−2921.
(9) Tatsuma, T.; Saitoh, S.; Ohko, Y.; Fujishima, A. *Chem. Mater.* **2001**, *13*, 2838−2842.
(10) Tae Kwon, Y.; Yong Song, K.; In Lee, W.; Jin Choi, G.; Rag Do, Y. *J. Catal.* **2000**, *191*, 192−199.
(11) Keller, V.; Bernhardt, P.; Garin, F. *J. Catal.* **2003**, *215*, 129−138.
(12) Chen, C. C.; Fan, H. J.; Jang, C. Y.; Jan, J. L.; Lin, H. D.; Lu, C. S. *J. Photochem. Photobiol., A* **2006**, *184*, 147−154.
(13) Chen, C. C.; Mai, F. D.; Chen, K. T.; Wu, C. W.; Lu, C. S. *Dyes Pigm.* **2007**, *75*, 434−442.
(14) Li, X.; Liu, G.; Zhao, J. *New J. Chem.* **1999**, *23*, 1193−1196.
(15) Garrido, M.; Larrechi, M. S.; Rius, F. X.; Tauler, R. *Chemom. Intell. Lab. Syst.* **2005**, *76*, 111−120.
(16) Garrido, M.; Lázaro, I.; Larrechi, M. S.; Rius, F. X. *Anal. Chim. Acta* **2004**, *515*, 65−73.
(17) Blanco, M.; Peinado, A. C.; Mas, J. *Anal. Chim. Acta* **2005**, *544*, 199−205.
(18) Fuerte, A.; Hernández-Alonso, M. D.; Maira, A. J.; Martínez-Arias, A.; Fernández-García, M.; Conesa, J. C.; Soria, J.; Munuera, G. *J. Catal.* **2002**, *212*, 1−9.
(19) Song, H.; Jiang, H.; Liu, X.; Meng, G. *J. Photochem. Photobiol., A* **2006**, *181*, 421−428.
(20) Eibl, S.; Gates, B. C.; Knözinger, H. *Langmuir* **2001**, *17*, 107−115.
(21) Djerad, S.; Tifouti, L.; Crocoll, M.; Weisweiler, W. *J. Mol. Catal. A: Chem.* **2004**, *208*, 257−265.
(22) Cordischi, D.; Gazzoli, D.; Occhiuzzi, M.; Valigi, M. *J. Solid State Chem.* **2000**, *152*, 412−420.
(23) Lebarbier, V.; Clet, G.; Houalla, M. *J. Phys. Chem. B* **2006**, *110*, 22608−22617.
(24) Di Paola, A.; García-López, E.; Marci, G.; Martín, C.; Palmisano, L.; Rives, V.; Venezia, A. M *Appl. Catal., B* **2004**, *48*, 223−233.
(25) Senthilkumaar, S.; Porkodi, K. *J. Colloid Interface Sci.* **2005**, *288*, 184−189.
(26) Sahoo, C.; Gupta, A. K.; Pal, A. *Dyes Pigm.* **2005**, *66*, 189−196.
(27) Ollis, D. F. *J. Phys. Chem. B* **2005**, *109*, 2439−2444.
(28) Emeline, A. V.; Ryabchuk, V. K.; Serpone, N. *J. Phys. Chem. B* **2005**, *109*, 18515−18521.
(29) Xu, Y.; Langford, C. H. *Langmuir* **2001**, *17*, 897−902.
(30) Marci, G.; Palmisano, L.; Sclafani, A.; Venezia, A. M.; Campostrini, R.; Carturan, G.; Martin, C.; Rives, V.; Solana, G. *J. Chem. Soc., Faraday Trans.* **1996**, 819−829.
(31) Martín, C.; Solana, G.; Rives, V.; Marci, G.; Palmisano, L.; Sclafani, A. *Catal. Lett.* **1997**, *49*, 235−243.
(32) Pan, J. H.; Lee, W. I. *Chem. Mater.* **2006**, *18* (3), 847−853.

(33) Chen, C.; Zhao, W.; Li, J.; Zhao, J.; Hidaka, H.; Serpone, N. *Environ. Sci. Technol.* **2002**, *36*, 3604−3611.
(34) Liu, G.; Li, X.; Zhao, J.; Hidaka, H.; Serpone, N. *Environ. Sci. Technol.* **2000**, *34*, 3982−3990.
(35) Cermenati, L.; Pichat, P.; Guillard, C.; Albini, A. *J. Phys. Chem. B* **1997**, *101*, 2650−2658.
(36) Chen, C.; Zhao, W.; Lei, P.; Zhao, J.; Serpone, N. *Chem.*−*Eur. J.* **2004**, *10*, 1956−1965.
(37) Chen, C. C.; Lu, C. S.; Chung, Y. C. *J. Photochem. Photobiol., A* **2006**, *181*, 120−125.
(38) Yang, J.; Chen, C.; Ji, H.; Ma, W.; Zhao, J. *J. Phys. Chem. B* **2005**, *109*, 21900−21907.
(39) Chen, C.; Li, X.; Ma, W.; Zhao, J.; Hidaka, H.; Serpone, N. *J. Phys. Chem. B* **2002**, *106*, 318−324.
(40) Chen, C.; Lei, P.; Ji, H.; Ma, W.; Zhao, J.; Hidaka, H.; Serpone, N *Environ. Sci. Technol.* **2004**, *38*, 329−337.